# Magneto Hydrodynamic Effect on Nanofluid Flow and Heat Transfer in Backward-Facing Step Using Two-Phase Model

F. Mobadersani[1]*, A. Rezavand[2]

[1] Faculty of Mechanical Engineering, Urmia University of Technology, Urmia, Iran.
[2] Mechanical Engineering Department, Université Laval, Quebec, Canada.

**ABSTRACT:** Magneto hydrodynamics effects on nanofluid flow in backward-facing step is studied using two-fluid model of Buongiorno. Due to the utilization of two-phase model, variable nanoparticle concentration and nanofluid properties are considered. Thermophoresis and Brownian diffusivities are calculated in particle dispersion. Effects of Reynolds number, particle volume fraction, magnetic field and Hartmann numbers are studied on heat transfer and fluid flow characteristics. It is shown that introduction of nanoparticles as a second phase, pushes reattachment point further into the downstream, while magnetic field has opposite effect and pushes it backward into the upstream. Particles are shown to be migrating from hot to cold regions due to the dispersion mechanisms considered. In comparison to single phase models, there is 3.7% decrease in maximum Nusselt number and more than 40% difference in the reattachment point location. Accuracy of the reattachment point is shown through previous pure fluid studies, the comparison to which show less than 0.8% tolerance with most recent studies. Relative effect of diffusion mechanisms is compared in different flow conditions, which show up to 12.5% difference. Application of magnetic field results in average Nusselt number increase of more than 10% by Hartmann number of 12.

## 1- Introduction

Increasing the efficiency of cooling and heating devices has always been of great importance among scientists. Furthermore, recent advances in technology and electronics have created higher demand in performance increase of those devices. Two separate categories of heat transfer enhancement mechanisms, namely active and passive methods, are utilized. Active methods require energy consumption for the additional heat transferred from surfaces. On the other hand, passive methods increase heat transfer without using additional energy. Choi and Eastman [1] used a passive method in which particles of Nano-size are added to the working fluid to alter thermal characteristics of the fluid and flow. This method that was later studied by many researchers [2-6] considerably increases heat transfer without significant change in the characteristics of the fluid. Murshed et al. [7] suggested that higher volume fraction of nanoparticles results in significantly higher Nusselt number and convective heat transfer coefficient. Their study is based on $TiO_2$-Water in laminar flow inside a tube.

Motion of electrically conducting fluid in a magnetic field, has created a new branch of hydrodynamics called Magneto Hydro-Dynamics (MHD). This new field has gained attention in recent years and is usually encountered in solar power technology, re-entry of space vehicles, astrophysical flows, blood flow measurements and electrical power generation. Motion of electrically conducing fluid in a magnetic field induces a current in the fluid, which produces a force called Lorentz force. Lorentz force is reported to reduce the fluid current field, which in turn, reduces the heat transfer rate in the flow [8,9]. Sheikholeslami et al. [10] showed that heat transfer rate decreases with augment of Lorentz forces in study of nanofluid free convective heat transfer. Rudraiah et al. [11] also showed that natural convection heat transfer rate decreases with magnetic field in rectangular enclosure. Kasaeipoor et al. [12] performed a numerical analysis on mixed convective heat transfer of nanofluid flow inside a T-shaped cavity in a constant magnetic field. They revealed that except two states, existence of nanoparticles enhances heat transfer rate. They also reported heat transfer improvement by increasing the cavity dimensions. Nanofluid flow in a rectangular channel, in the presence of a magnetic field, was analyzed by Heidary et al. [13]. They reported 75% enhancement in convective heat transfer by increasing nanoparticle volume concentration. The study of nanofluid flow inside a C-shaped cavity in a magnetic field was performed by Mojumder et al. [14]. They demonstrated a significant heat transfer enhancement by increasing Rayleigh and decreasing Hartmann numbers. Higher heat transfer rates were also observed by increase in nanoparticle concentration. Significant decrease in entropy generation rates by application of a magnetic field is reported by Chamkha et al. [15]. Their study is based on natural convection in a C-shaped cavity that is filled with CuO-Water nanofluid. Cu-water nanofluid in a lid-driven cavity under mixed convection is studied by Ismael et al. [16]. Their results demonstrated that magnetic field orientation is a key control mechanism in convective

*Corresponding author's email: fmobdersani@gmail.com

heat transfer.

Due to the importance of separation in industrial and scientific applications [17-19], forward-facing and backward-facing steps are considered benchmark problems that are widely applied for different flow conditions. Experimental and numerical study of ethylene glycol-functionalized graphene nanoplatelets/water-ethylene glycol nanofluids are conducted by Amiri et al. [20]. Their results indicated that higher weight concentration improves heat transfer rates in backward-facing step. A review of nanofluid flow on corrugated facing steps has been presented by Mohammad et al. [21]. Numerical and experimental study of Nanofluid flow and heat transfer is reported by Kherbeet et al. [22]. Their single phase study includes bulk effect of Brownian motion of nanoparticles. Laminar convective nanofluid flow over a backward-facing step with elastic bottom wall is conducted by Selimefendigil and Oztop [23]. Buoyancy, thermal radiation and viscous dissipation have been neglected in their single phase, steady, two-dimensional and laminar model. They proved that the maximum and average Nusselt numbers are affected by the size and flexibility of the hot surface. In the single phase, finite volume method used by Abu-Nada [24], particle type and volume fraction effects are studied in a backward-facing step. The results indicate that higher volume fractions result in higher average Nusselt numbers.

Due to the limitations of computational resources and costs, most of the numerical studies are carried out in single phase or homogenous models. This method does not model the particles separately and only bulk effect of their addition is taken into account by merely changing the properties of the fluid. Thermal equilibrium and zero slip velocity between particles and the base fluid is assumed in single phase models. Traditionally derived pure-fluid-heat transfer correlation like Dittus-Boelter are assumed to be valid for nanofluid flows, provided that the properties of pure fluid is replaced by that of the nanofluid [25]. This deduction is due to the direct application of conventional transport equations in nanofluid flows. These assumptions result in uniform particle distribution and absence of particle dispersion and these in turn, results in loss of accuracy and conflict with experimental data. In these models, thermal conductivity is considered the only important parameter in increase of heat transfer. The assumption that besides thermal conductivity, particle dispersion also plays a role in heat transfer, gave another group of single phase models, which was first proposed by Xuan and Roetzl [26]. Their method utilized an emperical correlation to take particle dispersion into account and allows non-zero velocity between particles and the base fluid. The resulting relative velocity is treated in the form of perturbation of energy equation. Later it was shown that the share of dispersion in the heat transfer enhancement is negligible and the important factor is non-uniform properties of the nanofluid that is produced by non-uniform particle distribution [25]. Wen and Ding [27] also emphasized the importance of particle diffusion.

Nanoparticles are introduced to the base fluid as a second component and the zero slip assumption is not valid [28]. Thus a realistic model should calculate the flow in two separate phases. The gravity, Thermophoresis effect, Brownian motion and diffusion and sedimentation are the driving forces that produce a slip velocity between two phases.

The increased computational cost and required resources have greatly limited the use of different two-phase models including Eulerian-Lagrangian and Eulerian-Eulerian; the latter of which itself has three different models namely, mixture, Volume Of Fluid (VOF) and Eulerian. As a different method proposed by Buongiorno [25] has advantages of all these methods and lacks their disadvantages. It is a two-fluid (nanoparticles and base working fluid), four-equation, non-homogenous, equilibrium model; which includes different dispersion mechanisms and calculates the non-uniform particle concentration. Successful application of this two-fluid model is presented by Bahiraei et al. [29] for heat transfer and particle migration studies in a pipe. The results of an annulus in a magnetic field that has been presented by Sheikholeslami and Abelman [30] indicate that Hartman number and aspect ratio are directly related to the Nusselt number. On the other hand, Schmidt-, Reynolds and Eckert- number and Brownian and thermophoresis parameters are indirectly related to the Nusselt number. Sheikholeslami et al. [31] studied effects of thermal radiation on magneto hydrodynamics flow and heat transfer between two parallel plates by means of this two-phase model. The dispersion mechanisms of this study include Brownian motion and thermophoresis effects.

The current work has been motivated by the lack of data from two-phase models in the literature. Buongiorno's two-fluid model is used in the calculation of heat transfer and particle distribution on a backward-facing step that has been subjected to a uniform magnetic field. Continuity, momentum and energy equations along with a nanoparticle dispersion equation have been solved with magnetic field consideration. Mesh independency has been demonstrated using different grid sizes. Effects of different parameters including Reynolds number, Hartmann number and volume fraction of the particles have been investigated and the results are in agreement with the previous studies.

## 2- Governing Equations

A backward-facing step with steady state, incompressible, laminar, nanofluid flow that has been subjected to a uniform magnetic field is studied in this work. x-axis is assumed to be along the channel length and y-axis is along the step height. Total length of the channel is 48S, 13S of which is located in the upstream of the step and 35S is the length of the domain after the step location. Expansion ratio is held constant at the value of 2 throughout this study. Bottom wall in the downstream section is held at constant temperature of $T_w$ = 310 K. Inlet temperature of the nanofluid is constant at $T_{in}$ = 300 K.

Continuity, conservation of momentum, conservation of energy with a source term regarding dispersion of nanoparticles and conservation of nanoparticles are the governing equations in this study. Effects of uniform magnetic field are introduced by a source term in the momentum equation [25].

$$\rho_{nf}(\nabla.V) = 0 \tag{1}$$

$$\rho_{nf}(\nabla.V)V = \nabla.[-PI + \nabla.\mu_{nf}(\nabla.V)] + \sigma_{nf}(V \times B) \times B \tag{2}$$

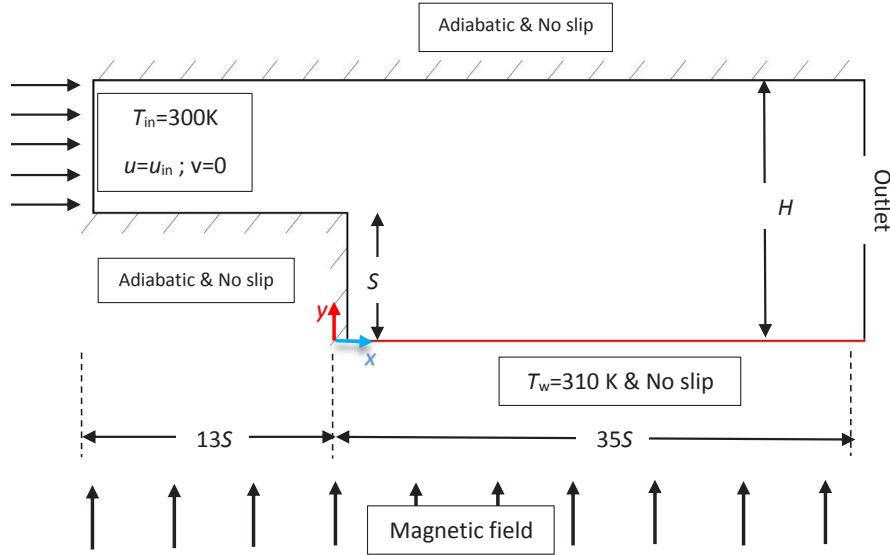**Fig. 1. Geometry**

$$(\rho C_p)_{nf} V.\nabla T + \nabla.(-k_{nf}\nabla T) = (C_p)_{np} J_{np}.\nabla T \qquad (3)$$

$$V.\nabla\phi = -\frac{1}{\rho_{nf}}\nabla.J_{np} \qquad (4)$$

The flux of nanoparticles, $J_{np}$, containing Brownian and thermophoresis terms is defined by $J_{np} = J_{np,B} + J_{np,T}$. The Brownian diffusivity, $J_{np,B}$, is calculated using Stokes-Einstein model [25], $J_{np,B} = -\rho_{np}D_B\nabla\phi$, where $D_B = \frac{K_B T}{3\pi\mu_f d_{np}}$. Thermophoretic diffusivity, $J_{np,T}$, is defined by McNab-Meisen [32] approximation for dispersed nanoparticles relative velocity in a liquid, as $J_{np,T} = -\rho_{np}D_T\nabla T$, where $D_T = 0.26\frac{k_f}{2k_f + k_{np}}\frac{\mu_f}{T\rho_f}\phi$.

Due to the dependency of energy and momentum, Eqs. (2) and (3), on nanofluid properties, the properties should be recalculated in every sequence. This allows the inclusion of the effects of volume fraction changes on nanofluid properties. In the calculation of nanofluid viscosity, dilute suspension of fine spherical particles is assumed. Therefore, the viscosity, density and heat capacity equations suggested by Brinkman are used [33].

On the other hand, the effective thermal conductivity is calculated using the relation presented by Khanafer et al. [34].

And the effective electrical conductivity of the nano fluid is approximated by Maxwell-Granetts (MG) model [33,34]:

$$\frac{\sigma_{nf}}{\sigma_f} = 1 + \frac{3(\sigma_{nf}/\sigma_f - 1)\phi}{(\sigma_{nf}/\sigma_f + 2) - (\sigma_{nf}/\sigma_f - 1)\phi} \qquad (5)$$

Dependency of the physical properties of nanofluid on the volume fraction, brings the essence of simultaneous solution of the governing equations.

In order to present a comparison of Thermophoresis and Brownian diffusivity, a ratio of Brownian to thermophoretic diffusivities is defined as follows:

$$N_{BT} = \frac{-\phi T D_B}{D_T(\partial T/\partial y)H} \qquad (6)$$

Following non-dimensional numbers including Reynolds, Hartmann, local and average Nusselt numbers are defined and used for deriving the results:

$$Re = \frac{\rho_{nf}u_{in}D_H}{\mu_{nf}} = \frac{\rho_{nf}u_{in}(2H)}{\mu_{nf}}$$

$$Ha = \frac{B(2H)}{\sqrt{\sigma_{nf}/\mu_{nf}}} \qquad (7)$$

$$Nu_x = \frac{\left.\frac{\partial T}{\partial y}\right|_{wall}(2H)}{(T_w - T_b)}$$

where the bulk temperature of the fluid domain is:

$$T_b = \frac{\int_0^H uT dy}{\int_0^H u dy} \qquad (8)$$

The nanofluid enters the domain with uniform volume fraction, temperature value of 300 K and constant velocity, the value of which is calculated by Reynolds number. The volume fraction is assumed to be 2% unless otherwise stated.

Zero gradient boundary condition for the velocity and temperature velocity profiles are applied at the outlet. So, particle diffusion flux is assumed to be zero at the outlet.
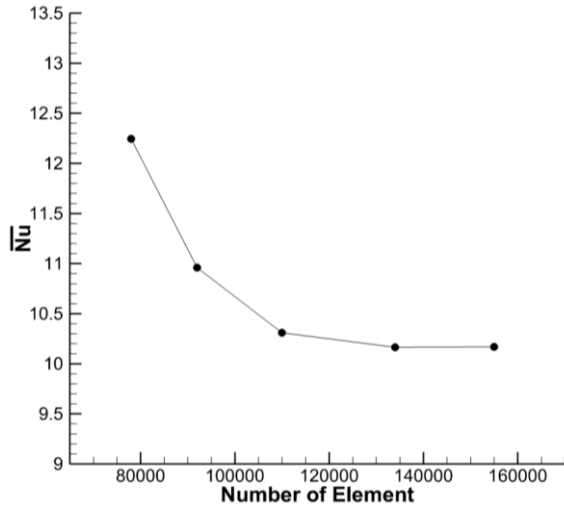
**Fig. 2. Mesh Independency**

Furthermore, no-slip boundary condition is applied on the walls. The temperature of the hot wall is held constant at 310 K, while all other walls are under adiabatic condition. Thus, the boundary conditions will be:

$$-n.(D_B \nabla \phi + D_T \nabla T) = 0 \, ,$$

$$-n.q = 0 \, , \qquad \frac{\partial u}{\partial x} = \frac{\partial v}{\partial x} = 0$$

$$u = v = 0 \, , \qquad T = T_w \quad \text{(on the hot wall)} \tag{9}$$

and $\quad q = 0$ (on the other walls)

As suggested by Sverre et al. [35], volume fraction boundary condition on the walls is set by the following equation:

$$-n.(D_B \nabla \phi + D_T \nabla T + V \phi) = 0 \tag{10}$$

## 3- Solution Method and Validation

The Galerkin weighted residual finite element method has been used to solve presented governing equations (Eqs. (1) to (4)) with boundary conditions (Eqs. (9) and (10)). Correction of the calculated field variables and forcing the residual to be zero over the computational domain is performed utilizing weighted functions.

$$\int_\Omega wf(x)Rd\omega = 0 \tag{11}$$

where wf, R, $\omega$ and $\grave{U}$ are weight function, residual, location variables and entire domain, respectively. Using weighted residual scheme, governing Partial Differential Equations (PDEs) are reduced to integral equations, which are then solved in a matrix by the Newton-Raphson iteration technique. The relative error for each field variable ($\Gamma$) should satisfy:

$$\left| \frac{\Gamma^{n+1} - \Gamma^n}{\Gamma^{n+1}} \right| < 10^{-5} \tag{12}$$

In which n denotes iteration. The velocity components and pressure are discretized using $P_2$-$P_1$ Lagrange finite elements. The grid consists of non-uniform triangular elements, which are finer in the vicinity of the walls to increase accuracy at locations of higher quantity gradients.

Fig. 2 presents the results of grid dependency analysis for five different mesh sizes. The comparison shows that the simulation becomes grid-independent at element number of 134000. This mesh is chosen as the appropriate mesh for the rest of this study, which keeps the number of elements in the minimum required value.

First, as presented in Table 1, benchmark results for pure water are used for validation. The table shows a minimum tolerance of 0.40% and about 0.60% error with the most recent studies in determination of the reattachment point. The best accuracy is achieved in comparison to Acharya et al. [36], the error of which is -0.4%.

The next step in the validation of the model is the accuracy of heat transfer and nanofluid flow, for which two different studies are utilized. Fig. 3 presents the validation of nanofluid flow and heat transfer phenomena using experimental data from Bahiraei et al. [41]. This figure reports convective heat

**Table 1. Reattachment length error compared to previous studies**

| Study | Solution method | Working fluid | $X_r/S$ | Error |
|-------|-----------------|---------------|---------|-------|
| Present study | Finite element | Pure water | 4.95 | 0.00% |
| Selimefendigil, Oztop [36] | Finite element | Pure water | 4.98 | -0.60% |
| Acharya et al. [35] | Finite difference | Pure water | 4.97 | -0.40% |
| Lin et al. [37] | Finite difference | Pure water | 4.91 | 0.80% |
| Dyne et al. [38] | Finite difference | Pure water | 4.89 | 1.20% |
| El-Refaee et al. [39] | Finite volume | Pure water | 4.77 | 3.77% |
| Cochran et al. [40] | Finite element, volume & difference | Pure water | 5.32 | -6.95% |
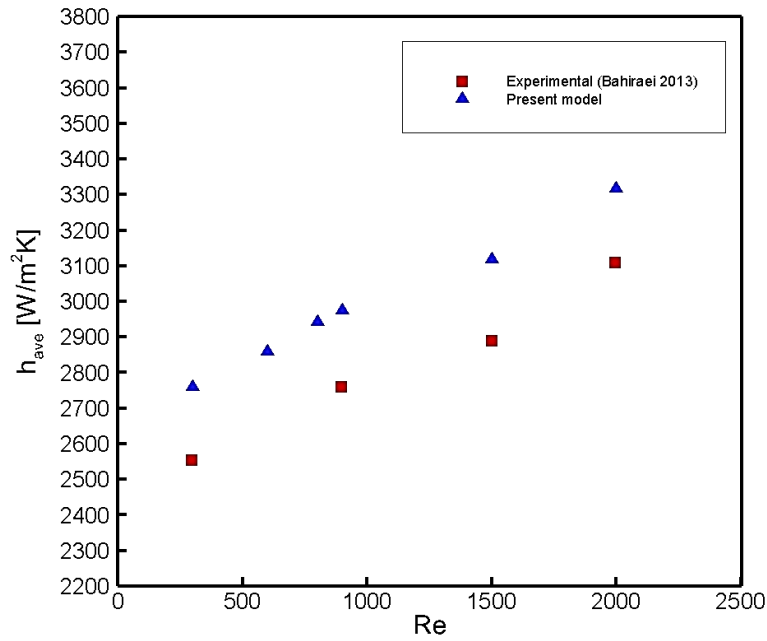
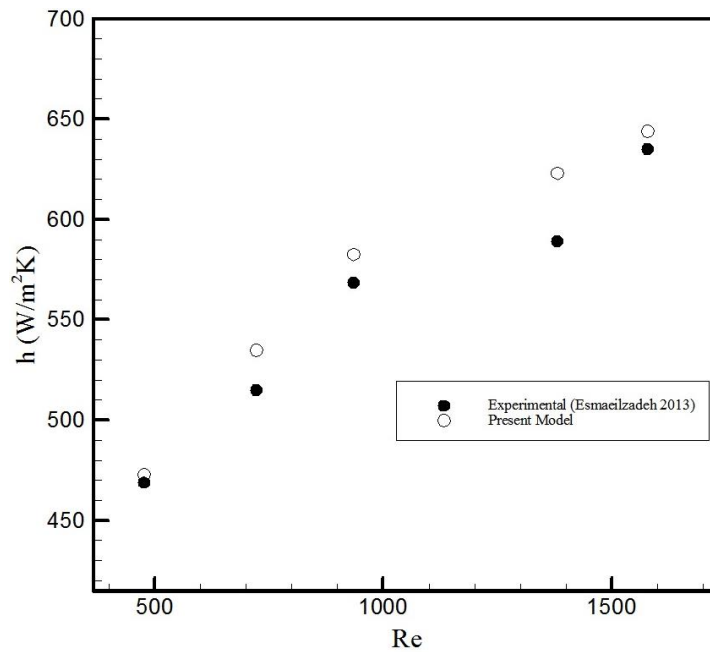**Fig. 3. Convective heat transfer coefficient of the nanofluid in pipe**



**Fig. 4. Validation of results with experimental data for Al2O3 in a horizontal tube**

transfer coefficient in axisymmetric nanofluid flow in a pipe with constant heat flux. The error between this study and the above mentioned experimental study is about 8%, which is an acceptable value for difference between numerical and experimental studies.

Experimental data for $Al_2O_3$-water laminar flow inside a horizontal tube with constant heat flux has been reported by Esmaeilzadeh et al. [42]. Comparison of local heat transfer coefficient for different Reynolds numbers between their study and the present model are presented in Fig. 4. The data are for heat flux of 9000 W/m², volume fraction of 0.5% and

the dimensionless distance from the inlet of pipe (x/d) of 56.86. Good agreement between these two data sets is evident in this figure.

Abu-Nada [24] studied single phase backward facing step and reported Nusselt number for a constant temperature hot wall. Error! Reference source not found. depicts comparison of those values with current study.

As a result of the stagnation point created by the impingement jet, the maximum Nusselt number is located at the reattachment point in both models. There are two differences between these two models, including maximum
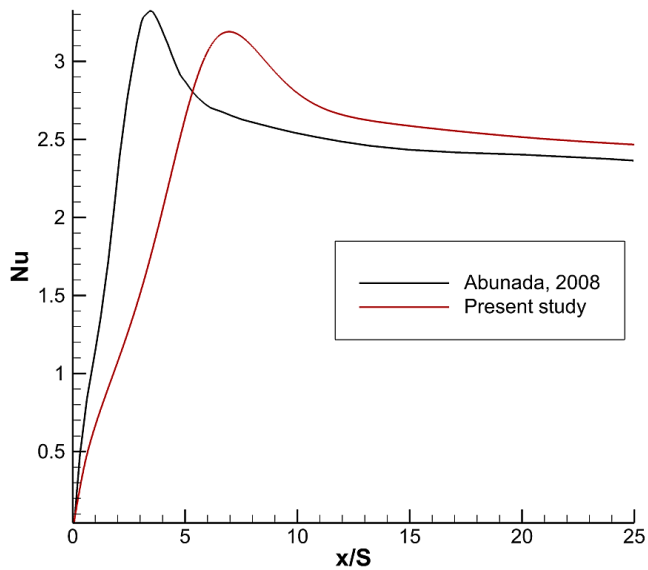
**Fig. 5. Nusselt number compared to the single phase model of Abunada [24]**

**Table 2. Properties of the base fluid and nanoparticles**

| Property | Pure water | Cu |
|---|---|---|
| $\rho$ (kg/m³) | 997.1 | 8933 |
| $\mu$ (N.m/s) | 1e-3 | - |
| $k$ (W/m.K) | 0.613 | 401 |
| $C_p$ (kJ/kg.K) | 4179 | 385 |
| $\sigma(1/\Omega m)$ | 0.05 | 5.96e7 |
| $d$ (m) | - | 98e-9 |

Nusselt number and the location of reattachment point. There is an accumulation of particles at the reattachment point in the physics of the flow, while single phase studies are unable to detect it. This accumulation causes an increase in the value of the thermal conductivity which in turn causes a reduction in the maximum Nusselt number. Absence of this phenomenon, dispersion of nanoparticles and their relative velocity with the base fluid in single phase studies result in slightly higher maximum Nusselt number.

On the other hand, difference in the reattachment location causes variations in the location of maximum Nusselt point. An error value of about 0.60% for reattachment point determination, in comparison to the most recent studies, has been presented in Table 1 and Abunada's statement regarding underestimation of the reattachment point in his work, it seems that the present work gives a better estimation of this point. Furthermore, in agreement with the previous studies, the single phase model gives a lower estimation of the average Nusselt number than two-phase models, which shows inadequacy of those models in heat transfer studies.

## 4- Results

Table 2 presents the properties of the base fluid and nanoparticles in this study. The Cu nanoparticles are used for the following nanofluid simulations.

In this section effects of particle distribution and presence of particle diffusion are studied. These effects cannot be detected by single phase models. Effects of presence of the magnetic field and Reynolds number on heat transfer values and particle distribution have also been presented.

Fig. 6 shows velocity contours in the recirculation zone for different Hartmann numbers. The inlet volume fraction and Reynolds number are 2% and 533, respectively. The origin of the x-axis is assumed to be at the inlet of the channel for this figure.

As the fluid particles reach top of the step, sudden area enlargement causes to their sharp velocity reduction and consequently rapid pressure increase. Resistance of the high

pressure downstream against the fluid particles cause to the formation of primary recirculation zone on the lower wall.

The velocity contours clearly show that recirculation zone is downsized by increase in the magnitude of the electromagnetic forces. This is due to the braking effect of the Lorentz force, which weakens the flow momentum. Thus, when the Ha is larger, the fluid particles will move with lower velocity that leading to small diverse pressure and consequently, small recirculation zone. Additionally, by developing progressively of the primary recirculation zone on the lower wall (in high momentum flows), the streamlines convex leading to an adverse pressure gradient along the upper wall. This phenomenon cause to a secondary recirculation zone on the top wall. By intensification of the applied magnetic field, the momentum of the fluid particles in the channel longitudinal direction will be weakened and consequently the secondary recirculation zone will be downsized.

Fig. 7 reports the local Nusselt number on the hot wall for different Reynolds numbers. In this figure, Hartmann number and volume fraction of the nanoparticles are set to 8 and 2%, respectively. As reported in this figure, increase in Reynolds number pushes the recirculation zone forward and increases its size. This in turn, pushes the location of maximum Nusselt number forward into the downstream. Furthermore, increase of average, local and maximum Nusselt numbers is clearly evident in this figure. Thus, increase in Reynolds number increases convective heat transfer and creates better heat transfer capabilities in backward-facing step.

Fig. 8 illustrates the effect of magnetic field intensity on the local and average Nusselt numbers. Different Hartmann numbers, in the range of 0 < Ha < 12 are considered in this figure. It can be observed in this figure that increase in the magnitude of the electromagnetic force and as a result in Hartmann number, increases the maximum and average Nusselt numbers and pushes the location of maximum Nusselt number further into the downstream section. Change of the average Nusselt number amounts to 10% by Hartmann number of 12. Furthermore, it can be seen that in lower Ha numbers, the amount of change in average Nu number is very small compared to larger Ha numbers. Reynolds number is set to 533 and volume concentration is 2% for this figure. The reason for this change in Nusselt number is that stronger magnetic field reduces flow momentum and this in turn changes the angle of collision of the incoming jet and hot wall. That is, the jet collides with an angle closer to the normal direction to the wall and recirculation region shrinks in size. This can be visualized in the contours of Fig. 6. This
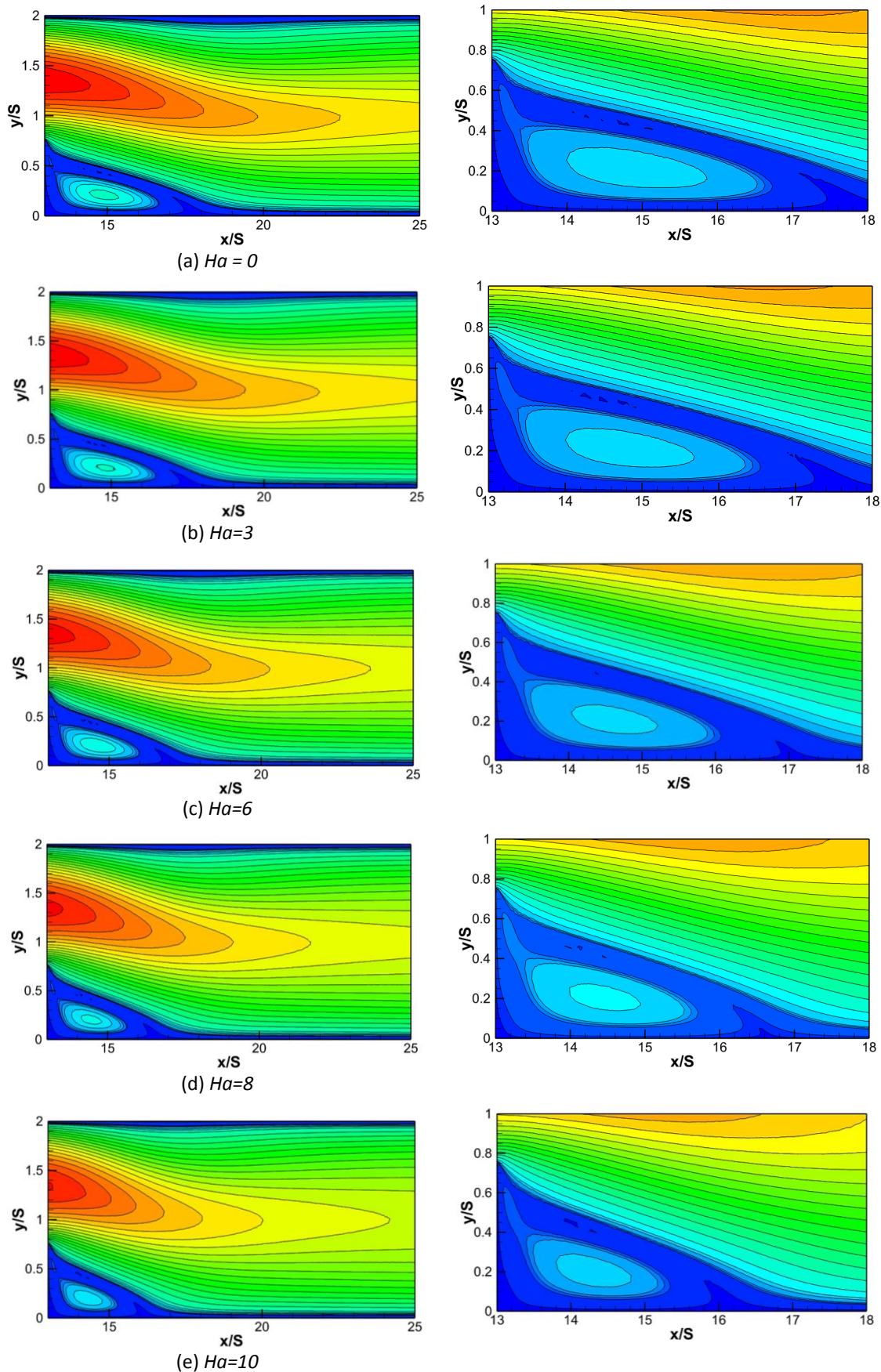
(a) *Ha = 0*

(b) *Ha=3*

(c) *Ha=6*

(d) *Ha=8*

(e) *Ha=10*

**Fig. 6. Velocity contours for different Hartmann numbers, Re=533,  :   Left side) after the step;   Right side) Close up view**
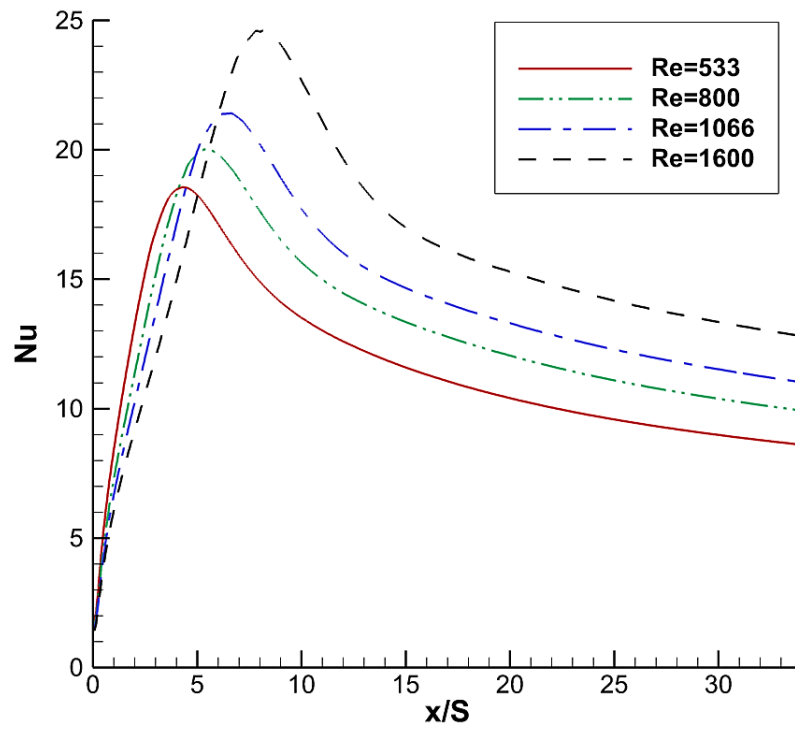
**Fig. 7. Local Nusselt number for different Reynolds numbers, Ha=8, $\phi = 2\%$ .**
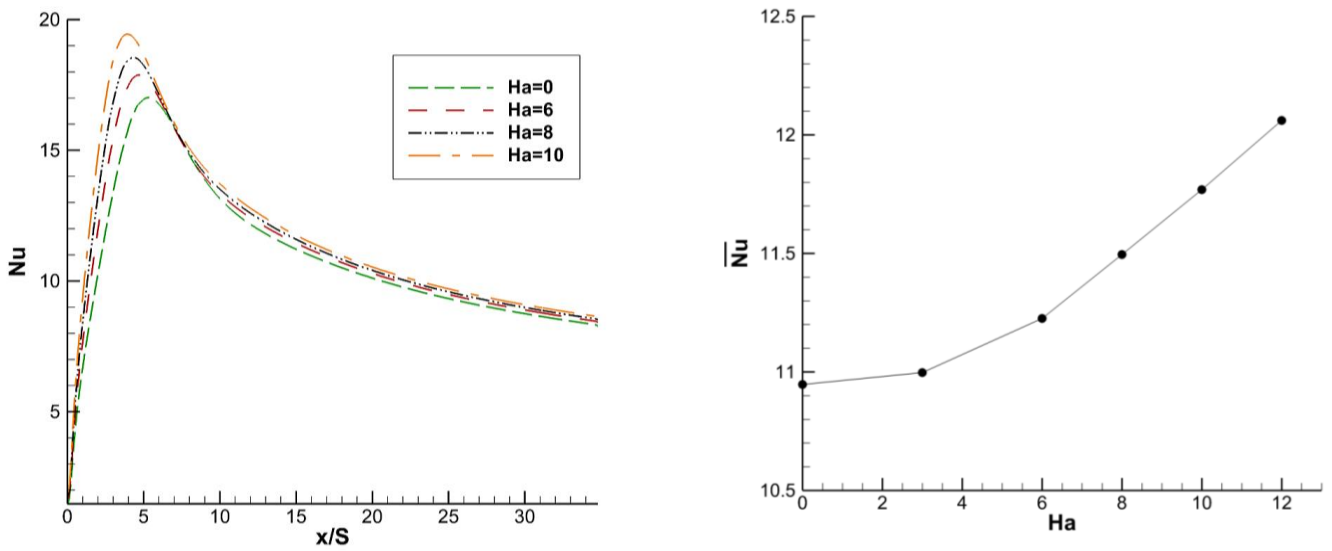


**Fig. 8. Local (left) and average Nusselt (right) numbers for different Hartmann numbers, Re=533, $\phi = 2\%$ .**
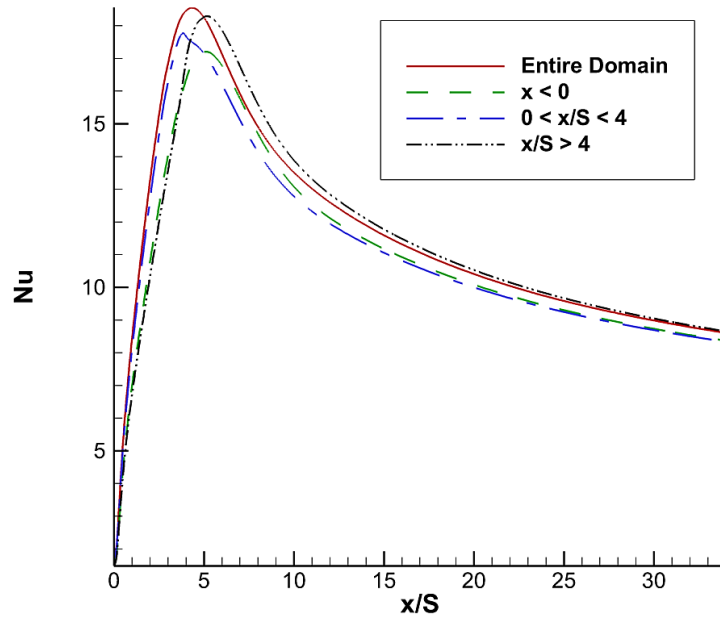
**Fig. 9. Nusselt number for various magnetic field locations; Re=533, $\phi = 2\%$ , Ha=8**
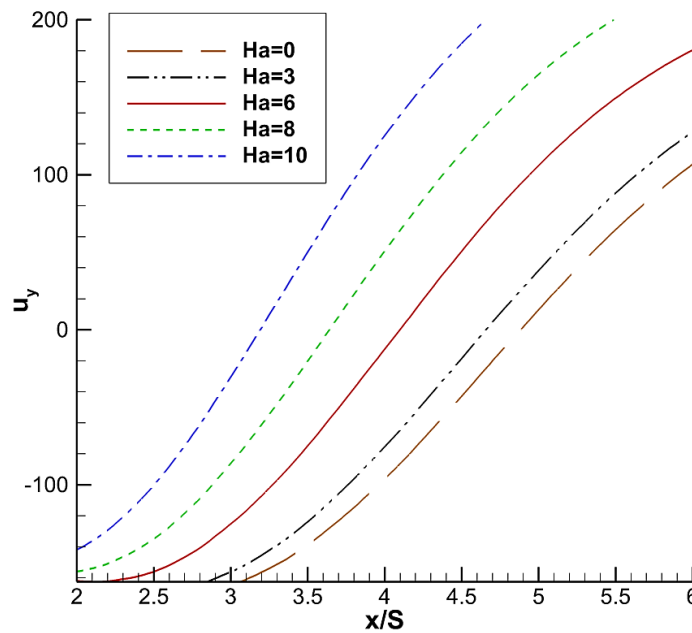


**Fig. 10. Effect of Hartmann number on reattachment point; Re=533, $\phi = 2\%$ .**

change in the collision angle and the size of the recirculation zone results in larger convective heat transfer.

Fig. 9 gives the Nusselt number for different locations of application of the magnetic field. Four different positions are considered including, before the step, between step and reattachment point, after the reattachment point and the entire domain. This figure illustrates the importance of magnetic field application in the recirculation region for the size of the region and the reattachment point. Presence of magnetic field at that location results in contraction of its size, while application of the magnetic field in locations other than

this region, has no significant effect on the size. Magnetic force effect before the step considerably decreases the flow momentum and its comparison with a case of the same reattachment point (x/S>4) shows that decreased momentum results in lower Nusselt number. On the other hand, comparing x/S<0 with the entire domain magnetic field indicates that maximum Nusselt number has a lower value for x/S<0. This can be attributed to the reattachment point location. When this point is closer to the wall, the impingement jet is stronger and creates larger Nu.

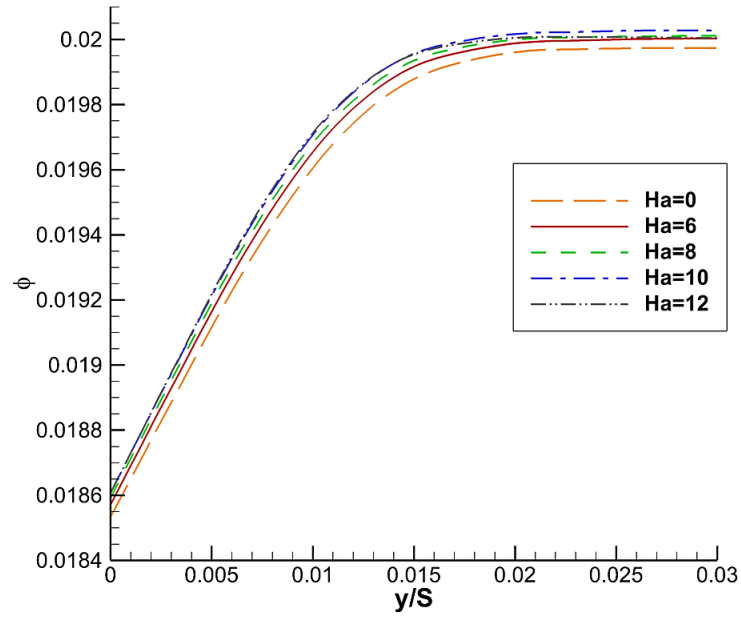Fig. 10 depicts $u_y$ for different Hartmann numbers and

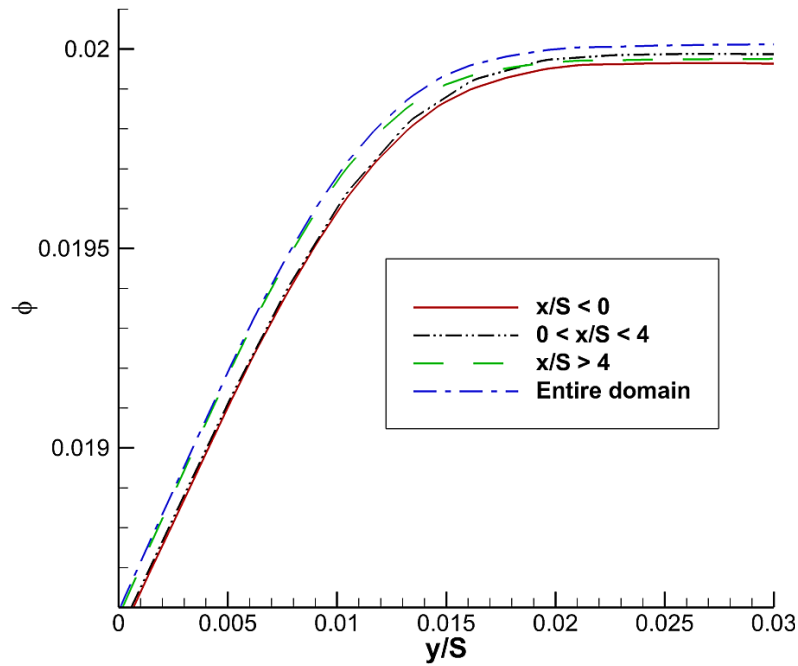**Fig. 11. Particle volume fraction in different magnetic field intensities; Re=533,** $\phi = 2\%$ **.**



**Fig. 12. Particle volume fraction at different positions of application of the magnetic field, Re=533,** $\phi = 2\%$ **, Ha=8.**

shows the location of reattachment point for different magnetic field intensities. This figure indicates that increase in the magnitude of electromagnetic forces pushes the reattachment point ($u_y$=0) back into the upstream and tends to downsize the recirculation zone. This behavior can be attributed to the decreased momentum magnitude in presence of larger electromagnetic forces.

Effect of Hartmann number on the distribution of nanoparticles is presented in Fig. 11 This figure indicates that higher values of magnetic field intensity slightly pushes the

nanoparticles into the wall, creating slightly higher particle distribution gradients. Thus, as can be seen in Fig. 8, this leads to increased maximum and average Nusselt numbers.

Effect of variations of magnetic field position on particle distribution profile is presented in Fig. 12. Reynolds, Hartmann number and inlet volume concentration are 533, 8 and 2%, respectively. Since the line on which the particle distribution is plotted is located at the downstream of the reattachment point, this figure shows that incase the magnetic field is applied at the location of interest, the particles are pushed
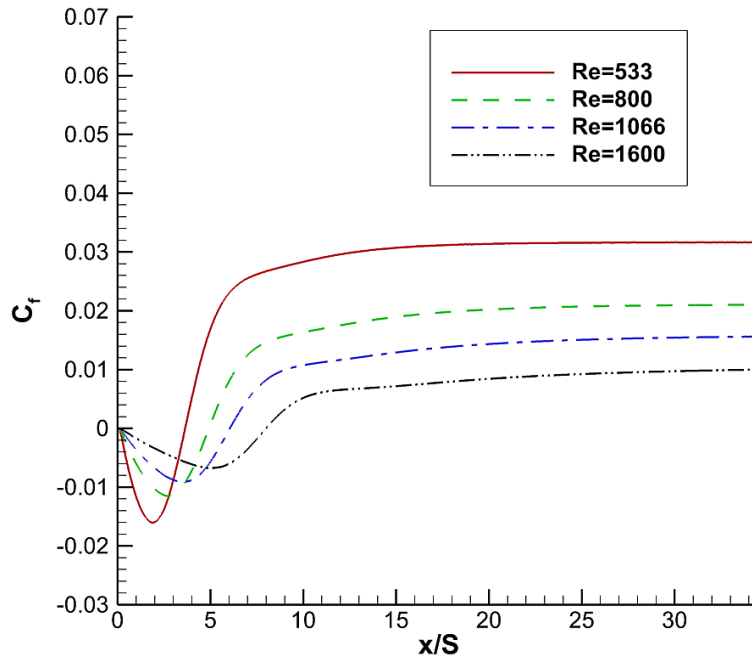
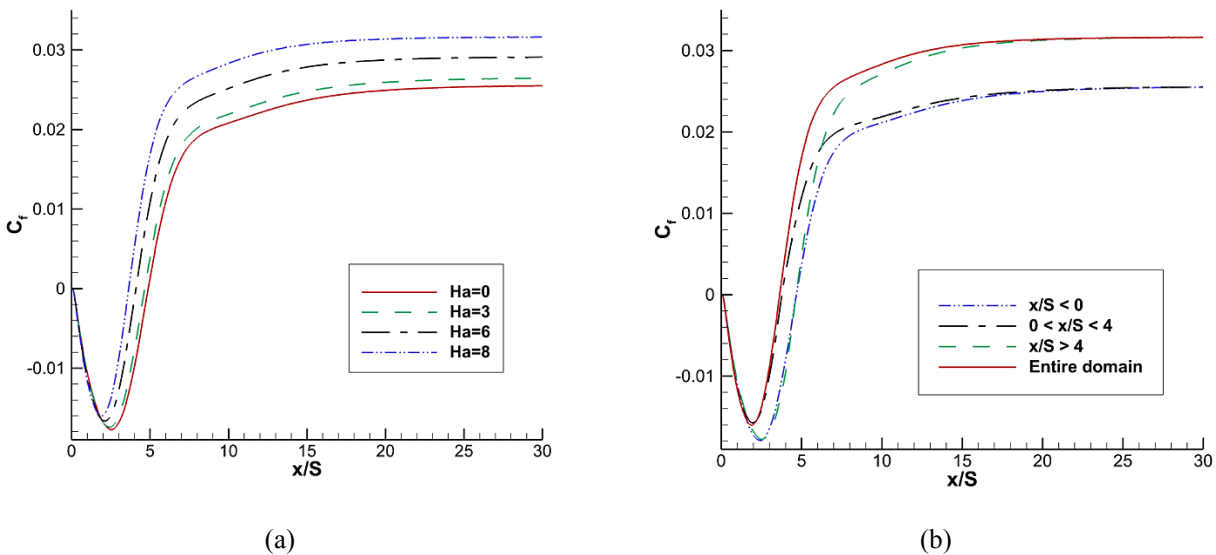**Fig. 13. Effects of Reynolds number on the skin friction coefficient, $\phi = 2\%$, Ha=8.**



         (a)                            (b)

**Fig. 14. Effect of the magnitude and position of magnetic field on skin friction coefficient Re=533, φ=2%; (b): Ha=8**

into the wall at that location. Otherwise, particle distribution near the wall is unaffected by location of magnetic forces.

Fig. 13 shows effect of Reynolds number on skin friction coefficient on the hot wall of backward facing step. Ha and $\phi$ are 8 and 2%, respectively. It can clearly be seen that higher Reynolds numbers rise shear tension and consequently skin friction coefficient. Presence of step causes formation of a vortex, which is responsible for negative friction coefficients that are due to negative velocity gradient at that zone. The absolute values of velocity gradient at that zone is smaller

than that of the rest of the channel, which gives lower absolute friction coefficients at the recirculation zone. Reduction in value of the coefficient as we approach to the reattachment point is because the fluid is pushed into the wall at that point and horizontal velocity component is reduced at that point.

Fig. 14 illustrates the effect of magnetic field on the skin friction coefficient. In both figures the inlet volume fraction is 2% and Reynolds number is 533. Ha number is set to 8 in Fig. 14(b). Fig. 14(a) shows the effect of magnetic field intensity. Furthermore, Fig. 14(b) depicts effects of the
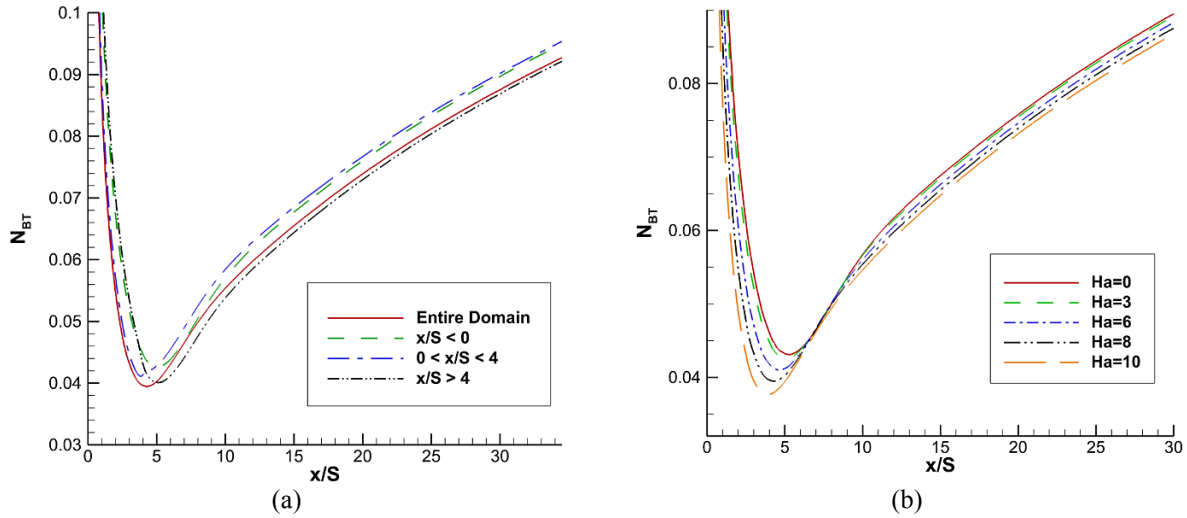
**Fig. 15. NBT at different positions and magnitudes of the magnetic field Re=533, $\phi = 2\%$ ; (a): Ha=8**

position of the magnetic field on skin friction coefficient. As can be seen in these figures, increase in the magnitude of the magnetic field pushes the reattachment point and minimum skin friction point backward, into the upstream and increases the shear tension and skin friction coefficient. Increase in fully developed region's $C_f$ can be attributed to the increased velocity gradient at that region in higher magnetic fields. The magnitude of changes by change of Ha number is nonlinear as shown in Fig. 14(a). Fig. 14(b) indicates that the responsible mechanism for increase of shear tension after the reattachment point, is application of magnetic field after that position only. Any region, to which magnetic forces are applied, experiences increase in shear tension. Additionally, it reports that change in the maximum friction coefficient at recirculation zone can only be done by application of magnetic field at recirculation zone. When the position of application is before or after that region, the zone is unaffected by the magnetic field.

The ratio of Brownian to thermophoretic diffusivity ($N_{BT}$) for different positions of the application and intensities of the magnetic field is depicted in Error! Reference source not found.. Two of the most important diffusion mechanisms that are responsible for the volume concentration change in different sections, are Brownian and thermophoresis diffusions. Random motion of particles is called Brownian motion and its value decreases in higher particle volume fractions. On the other hand, migration of particles from regions of higher temperature to regions of lower temperature is the effect of thermophoresis diffusion. The study of $N_{BT}$ gives useful information about the diffusion mechanism in nanofluid flows. Error! Reference source not found. shows that with increase in the portion of application of the magnetic field, Brownian diffusion decreases around reattachment point. After the reattachment position, in case the magnetic field is applied at that region, Brownian diffusion is reduced compared to thermophoretic diffusion.

As suggested by Fig. 15(b), higher intensities of the magnetic field result in larger thermophoretic diffusivity in comparison to Brownian diffusivity. Thus in larger Hartmann

numbers, thermophoretic effect gains more importance in diffusion of nanoparticles.

Demonstration of the presence of the recirculation zone is illustrated in Fig. 16, where velocity profiles at different locations of the recirculation zone are plotted. Volume fraction, Reynolds and Hartmann numbers are 2%, 533 and 10, respectively. At x/S=3.2 the reattachment point and zero gradient of the velocity profile on the wall are clearly observed. The velocity has a positive value in all points on this line. x/S=2.2 and 1.2 are located in the vortex zone. The negative values for the horizontal velocity show the presence of a vortex. Finally, the x/S=0.2 is in the vicinity of the step, where wall effects dominate in the velocity profile. Presence
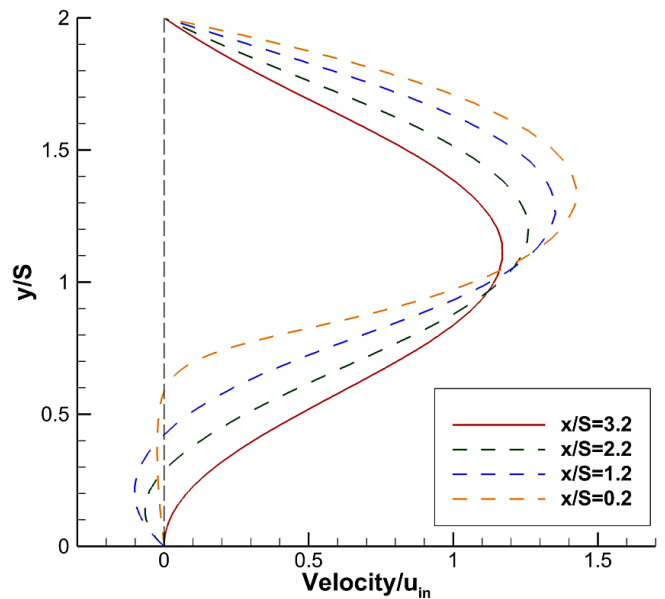


**Fig. 15. Velocity profile at the recirculation zone, Re=533, $\phi = 2\%$ , Ha=10**

of no-slip boundary condition on the wall has limited the velocity to a value near zero at this region. Decrease in the peak velocity as the flow moves downstream can clearly be visualized and the reason of this loss of energy is the expanded geometry at the step and also viscous losses.

## 5- Conclusion

Application of uniform magnetic field to backward-facing step with nanofluid flow is presented in this paper. As the advantage of two-phase models, particle distribution and dispersion effects are taken into account and the results are validated using different experimental and numerical studies. Since single phase models neglect non-uniform particle distribution, a very important part of the physics of the flow is not present in those models and they lack the required accuracy in heat transfer estimation. Particle accumulation at the reattachment point causes a higher conductivity which yields in lower maximum Nusselt number in two-phase models. Increase in Reynolds number, increases maximum and average Nusselt numbers and skin friction coefficient. Furthermore, it pushes the reattachment point and maximum Nusselt number further into the downstream. Higher Hartmann numbers downsizes the recirculation zone, pushes the reattachment point backward into the upstream, pushes nanoparticles into the hot wall and increases the Nusselt number. Additionally, absolute value of skin friction coefficient increases non-linearly with Ha number. Changes in the position of application of the uniform magnetic field has a very significant effect on the behavior of shear tension, particle distribution and Nusselt number and the ratio of Brownian to thermophoretic dispersion. Increase in the intensity of the uniform magnetic field reduces the share of Brownian diffusivity relative to thermophoretic diffusivity in nanoparticle diffusion.

| Nomenclature | | | |
|---|---|---|---|
| $B$ | Magnetic field, Tesla | **Greek symbols** | |
| $c_p$ | Specific heat, J/kg.K | $\mu$ | Viscosity, Pa.s |
| $d$ | Diameter, m | $\rho$ | Density, kg/m$^3$ |
| $D_B$ | Brownian diffusion coefficient | $\sigma$ | Electrical conductivity, 1/($\Omega$m) |
| $D_H$ | Hydraulic Diameter ($2H$) | | |
| $D_T$ | Thermal diffusion coefficient | $\phi$ | Nanoparticle volume fraction |
| $J$ | Mass flux, kg/m$^2$.s | | |
| $k$ | Thermal conductivity, W/m.K | **Subscripts** | |
| $K_B$ | Boltzman constant, J/K | | |
| $h$ | convective heat transfer coefficient, W/m$^2$.K | $b$ | bulk |
| | | $f$ | Base fluid |
| $H$ | Height of downstream m | $in$ | Inlet |
| $Ha$ | Hartmann number ($BD_H\sqrt{\sigma/\mu}$) | $nf$ | nanofluid |
| $L$ | Length, m | $np$ | Nanoparticle |
| $N_{BT}$ | Ratio of Brownian to thermophoretic diffusivity | $r$ | Reattachment |
| $Nu$ | Nusselt number ($h.D_H/k$) | $T$ | thermal |
| $P$ | Pressure, Pa | $w$ | Wall |
| $Q$ | Heat rate, W | | |
| $q''$ | Heat flux, W/m$^2$ | | |
| $Re$ | Reynolds number ($\rho u_{in}D_H/\mu$) | | |
| $S$ | Step height, m | | |
| $T$ | Temperature, K | | |
| $T_w$ | Wall temperature, K | | |
| $u$ | Velocity($x$-component), m/s | | |
| $v$ | Velocity($y$-component), m/s | | |
| $V$ | Velocity vector, m/s | | |
| $x$ | Distance, m | | |

## References

[1] S.U. Choi, J.A. Eastman, Enhancing thermal conductivity of fluids with nanoparticles, Argonne National Lab., IL (United States), 1995.

[2] M. Bahiraei, A comprehensive review on different numerical approaches for simulation in nanofluids: traditional and novel techniques, Journal of Dispersion Science and Technology, 35(7) (2014) 984-996.

[3] W.-S. Han, S.-H. Rhi, Thermal characteristics of grooved heat pipe with hybrid nanofluids, Thermal Science, 15(1) (2011) 195-206.

[4] G. Huminic, A. Huminic, I. Morjan, F. Dumitrache, Experimental study of the thermal performance of thermosyphon heat pipe using iron oxide nanoparticles, International Journal of Heat and Mass Transfer, 54(1-3) (2011) 656-661.

[5] N. Kannadasan, K. Ramanathan, S. Suresh, Comparison of heat transfer and pressure drop in horizontal and vertical helically coiled heat exchanger with CuO/water based nano fluids, Experimental Thermal and Fluid Science, 42 (2012) 64-70.

[6] R. Lotfi, A.M. Rashidi, A. Amrollahi, Experimental study on the heat transfer enhancement of MWNT-water nanofluid in a shell and tube heat exchanger, International Communications in Heat and Mass Transfer, 39(1) (2012) 108-111.

[7] S.S. Murshed, K.C. Leong, C. Yang, N.-T. Nguyen, Convective heat transfer characteristics of aqueous TiO 2 nanofluid under laminar flow conditions, International Journal of Nanoscience, 7(06) (2008) 325-331.

[8] A. Rashad, M.A. Ismael, A.J. Chamkha, M. Mansour, MHD mixed convection of localized heat source/sink in a nanofluid-filled lid-driven square cavity with partial slip, Journal of the Taiwan Institute of Chemical Engineers, 68 (2016) 173-186.

[9] M. Sathiyamoorthy, A.J. Chamkha, Natural convection flow under magnetic field in a square cavity for uniformly (or) linearly heated adjacent walls, International Journal of Numerical Methods for Heat & Fluid Flow, 22(5) (2012) 677-698.

[10] M. Sheikholeslami, T. Hayat, A. Alsaedi, MHD free convection of Al2O3–water nanofluid considering thermal radiation: a numerical study, International Journal of Heat and Mass Transfer, 96 (2016) 513-524.

[11] N. Rudraiah, R. Barron, M. Venkatachalappa, C. Subbaraya, Effect of a magnetic field on free convection in a rectangular enclosure, International Journal of Engineering Science, 33(8) (1995) 1075-1084.

[12] A. Kasaeipoor, B. Ghasemi, S. Aminossadati, Convection of Cu-water nanofluid in a vented T-shaped cavity in the presence of magnetic field, International Journal of Thermal Sciences, 94 (2015) 50-60.

[13] H. Heidary, R. Hosseini, M. Pirmohammadi, M. Kermani, Numerical study of magnetic field effect on nano-fluid forced convection in a channel, Journal of Magnetism and Magnetic Materials, 374 (2015) 11-17.

[14] S. Mojumder, S. Saha, S. Saha, M. Mamun, Effect of magnetic field on natural convection in a C-shaped cavity filled with ferrofluid, Procedia Engineering, 105 (2015) 96-104.

[15] A. Chamkha, M. Ismael, A. Kasaeipoor, T. Armaghani, Entropy generation and natural convection of CuO-water nanofluid in C-shaped cavity under magnetic field, Entropy, 18(2) (2016) 50.

[16] M.A. Ismael, M. Mansour, A.J. Chamkha, A. Rashad, Mixed convection in a nanofluid filled-cavity with partial slip subjected to constant heat flux and inclined magnetic field, Journal of Magnetism and Magnetic Materials, 416 (2016) 25-36.

[17] J.G. Barbosa-Saldaña, N. Anand, Flow over a three-dimensional horizontal forward-facing step, Numerical Heat Transfer, Part A: Applications, 53(1) (2007) 1-17.

[18] D. Barkley, M.G.M. Gomes, R.D. Henderson, Three-dimensional instability in flow over a backward-facing step, Journal of Fluid Mechanics, 473 (2002) 167-190.

[19] F. Selimefendigil, H.F. Öztop, Numerical analysis of laminar pulsating flow at a backward facing step with an upper wall mounted adiabatic thin fin, Computers & Fluids, 88 (2013) 93-107.

[20] A. Amiri, H.K. Arzani, S. Kazi, B. Chew, A. Badarudin, Backward-facing step heat transfer of the turbulent regime for functionalized graphene nanoplatelets based water–ethylene glycol nanofluids, International Journal of Heat and Mass Transfer, 97 (2016) 538-546.

[21] K.A. Mohammed, A.A. Talib, A. Nuraini, K. Ahmed, Review of forced convection nanofluids through corrugated facing step, Renewable and Sustainable Energy Reviews, 75 (2017) 234-241.

[22] A.S. Kherbeet, H. Mohammed, B. Salman, H.E. Ahmed, O.A. Alawi, Experimental and numerical study of nanofluid flow and heat transfer over microscale backward-facing step, International Journal of Heat and Mass Transfer, 79 (2014) 858-867.

[23] F. Selimefendigil, H.F. Öztop, Laminar convective nanofluid flow over a backward-facing step with an elastic bottom wall, Journal of Thermal Science and Engineering Applications, 10(4) (2018) 041003.

[24] E. Abu-Nada, Application of nanofluids for heat transfer enhancement of separated flows encountered in a backward facing step, International Journal of Heat and Fluid Flow, 29(1) (2008) 242-249.

[25] J. Buongiorno, Convective transport in nanofluids, Journal of heat transfer, 128(3) (2006) 240-250.

[26] Y. Xuan, W. Roetzel, Conceptions for heat transfer correlation of nanofluids, International Journal of heat and Mass transfer, 43(19) (2000) 3701-3707.

[27] D. Wen, Y. Ding, Effect of particle migration on heat transfer in suspensions of nanoparticles flowing through minichannels, Microfluidics and Nanofluidics, 1(2) (2005) 183-189.

[28] Y. Xuan, Q. Li, Heat transfer enhancement of nanofluids, International Journal of heat and fluid flow, 21(1) (2000) 58-64.

[29] M. Bahiraei, S. Mostafa Hosseinalipour, M. Hangi, Prediction of convective heat transfer of Al2O3-water nanofluid considering particle migration using neural network, Engineering Computations, 31(5) (2014) 843-863.

[30] M. Sheikholeslami, S. Abelman, Two-phase simulation of nanofluid flow and heat transfer in an annulus in the presence of an axial magnetic field, IEEE Transactions on Nanotechnology, 14(3) (2015) 561-569.

[31] M. Sheikholeslami, D.D. Ganji, M.Y. Javed, R. Ellahi, Effect of thermal radiation on magnetohydrodynamics

nanofluid flow and heat transfer by means of two phase model, Journal of Magnetism and Magnetic Materials, 374 (2015) 36-43.

[32] G. McNab, A. Meisen, Thermophoresis in liquids, Journal of Colloid and Interface Science, 44(2) (1973) 339-346.

[33] H. Brinkman, The viscosity of concentrated suspensions and solutions, The Journal of Chemical Physics, 20(4) (1952) 571-571.

[34] K. Khanafer, K. Vafai, M. Lightstone, Buoyancy-driven heat transfer enhancement in a two-dimensional enclosure utilizing nanofluids, International journal of heat and mass transfer, 46(19) (2003) 3639-3653.

[35] S.G. Johnsen, T.M. Pääkkönen, S. Andersson, S.T. Johansen, B. Wittgens, On the wall boundary conditions for species-specific mass conservation equations in mathematical modelling of direct precipitation fouling from supersaturated, multi-component fluid mixtures, arXiv preprint arXiv:1703.01448, (2017).

[36] S. Acharya, G. Dixit, Q. Hou, Laminar mixed convection in a vertical channel with a backstep: a benchmark study, ASME-PUBLICATIONS-HTD, 258 (1993) 11-11.

[37] F. Selimefendigil, H.F. Öztop, Effect of a rotating cylinder in forced convection of ferrofluid over a backward facing step, International Journal of Heat and Mass Transfer, 71 (2014) 142-148.

[38] J.-T. Lin, B.F. Armaly, T. Chen, Mixed convection in buoyancy-assisting, vertical backward-facing step flows, International Journal of Heat and Mass Transfer, 33(10) (1990) 2121-2132.

[39] B.R. Dyne, D.W. Pepper, F.P. Brueckner, Mixed convection in a vertical channel with a backward facing step: A benchmark problem, ASME-PUBLICATIONS-HTD, 258 (1993) 49-49.

[40] M. El-Refaee, M. Elsayed, N. Al-Najem, I. Megahid, Steady-state solutions of buoyancy-assisted internal flows using a fast false implicit transient scheme (FITS), International Journal of Numerical Methods for Heat & Fluid Flow, 6(6) (1996) 3-23.

[41] R. Cochran, R. Horstman, Y. Sun, A. Emery, Benchmark Solution for a Vertical, Buoyancy-Assisted Laminar Backward-Facing Step Flow Using Finite Element, Finite Volume and Finite Difference Methods, ASME-PUBLICATIONS-HTD, 258 (1993) 37-37.

[42] M. Bahiraei, S.M. Hosseinalipour, Thermal dispersion model compared with Euler-Lagrange approach in simulation of convective heat transfer for nanoparticle suspensions, Journal of Dispersion Science and Technology, 34(12) (2013) 1778-1789.

[43] E. Esmaeilzadeh, H. Almohammadi, S.N. Vatan, A. Omrani, Experimental investigation of hydrodynamics and heat transfer characteristics of γ-Al2O3/water under laminar flow inside a horizontal tube, International Journal of Thermal Sciences, 63 (2013) 31-37.